

Biological Basis of Medical Imaging

Literature Review of Medical Image Post-Processing Methods

Rocio Cabrera Lozoya, Mojdeh Rastgo Dastjerdi and Guillaume Lemaitre

Abstract— This report presents the research done on methods to image abdominal aortic aneurysm (AAA) and image post-processing methods in order to aid in the diagnose of the disease. Though ultrasound (US), computed tomography (CT) and magnetic resonance imaging (MRI) are the most commonly used imaging methods, this report will focus only on the use of CT and MRI images to diagnose AAA. Two image processing methods will be presented for CT images and two for MR images.

I. INTRODUCTION

An aneurysm is a vascular pathology consisting of an irreversible dilation of a segment of a blood vessel; it can be classified according to the location and configuration of the lesion [6]. The abdominal aorta is a continuation of the thoracic aorta and begins at the level of the diaphragm; it is the largest artery in the abdominal cavity. This major blood vessel can also suffer from diseases, including an abdominal aortic aneurysm (AAA). Figure 1 shows that AAAs appear as swellings of the blood vessel. In radiological studies, the diameter of a normal abdominal aorta is about 19 mm; an accepted criterion to diagnose an AAA defines it as a fifty percentage increase of the blood vessel diameter [6].

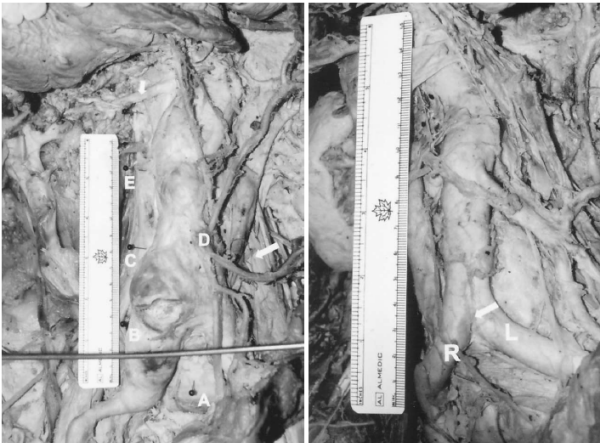


Fig. 1: Cadaveric specimens of the abdominal aorta. Left: Abdominal Aortic Aneurysm. Right: Normal Abdominal Aorta.

An AAA is developed when the balance between elastin and collagen fibres, important structural components of a blood vessel wall, is disturbed. In healthy subjects, elastin is responsible for the elastic recoil of the arteries due to the pulsatile blood flow [6]. Degradation

or loss of elastin fibres will then shift the load to the collagen fibres, decreasing the elasticity of the vessel and increasing its diameter, which in latter stages of the disease can lead to aortic rupture [6]. Genetic factors and environmental factors such as smoking and atherosclerotic disease contribute to the development of AAA; Figure 2 shows a schematic of the pathogenesis of abdominal aortic aneurysm [6].

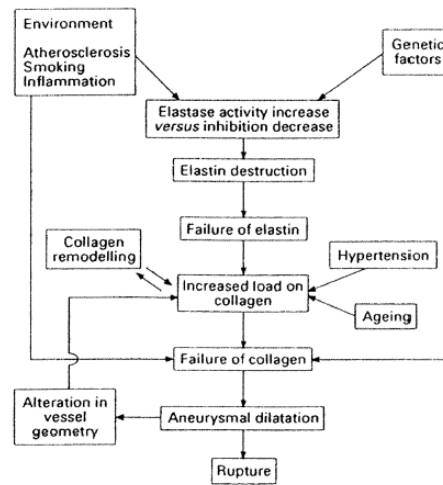


Fig. 2: Pathogenesis of an AAA.

It is of great clinical importance to be able to determine the abdominal aortic diameter in order to diagnose AAA and to appropriately plan a treatment or surgical intervention. Imaging techniques such as Computed Tomography and Magnetic Resonance Imaging are of great use to show the anatomical details of the diseased vessel. After image acquisition, image processing methods aim to accurately segment the vessel to be able to determine its dimensions. The following sections will describe some post processing algorithms currently developed in order to aid in AAA diagnosis.

II. COMPUTED TOMOGRAPHY IMAGING

Computed tomography (CT) and multi-detector computed tomography (MDCT) are the most known and used imaging techniques for evaluating aortic aneurysm. This is due to the fact that CT provides the best quality method for a detailed anatomical analysis of the aneurysm and adjacent arteries [18]. CT imaging speed is another advantage for this modality. Different post-processing methods such as volume

rendering, maximum intensity projection or multi-planar reformation can be used on the CT images in order to provide useful information for treatment planning and treatment of the lesions in and around the aneurysm wall. The information obtained from the CT images also highlights the three dimensional information which could be used for 3D reconstruction of aorta and its branches [18]. In general, CT is the best method for showing the aortic wall, which is of great importance in surgical planning. In some cases, it is also the most appropriate method for urgent patient evaluation; for instance in emergency cases, where it is used to predict aneurysm rupture [18].

III. CT IMAGE PROCESSING

In this document two post processing method based on computed tomography imaging are discussed. The first method is concerning segmentation and three dimensional reconstruction of AAA through a level based approach, while the second method uses active shape model in order to segment and construct the 3D model of the AAA.

A. AAA Segmentation through Level Set Methods

The level set method was used by Mageea et al. in order to segment the complex anatomical structure of AAA [13]. The method was used to provide better decisions for patients in order to proceed with endovascular repair of AAA. The proposed post processing method was performed on CT images. This section provides a brief overview of the proposed methods in [13].

A level set numerical method (LSM) could be used to track interfaces and shapes; this approach has been previously used for modelling the surface and objects in fluid mechanics and material science. Recently, it has been proved that it is also useful as a segmentation algorithm [13]. This method has the advantage of performing numerical computations for curves and surfaces on a fixed Cartesian grid without parametrizing the objects [15]. It also makes it easier to follow time varying object shapes while the object shape change topology [15]. Figure 3a [15] can be used to explain the general concept of level set method. The shape in Figure 3a shows the bounded region with well defined boundaries. This shape is determined with the level set function φ ; the red surface graph shows the level set function with reference to $x - y$ plane, which is shown with the blue surface [15]. The level set function φ is zero on the boundary of the shape and is positive for the shape itself. This means that shape is represented with set of points in the plane for which φ is positive or zero [15]. Figure 3b shows the same shape while it changes its topology by splitting to two parts. This shape is easier to represent

with level sets instead of using the shape directly [15].

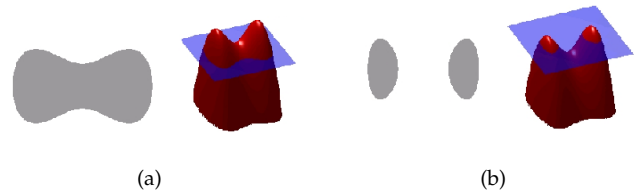


Fig. 3: Level set method illustration

Based on the level set explanation, it could be shown that this method represents a closed curve Γ using the level set function φ where Γ is the zero level set of φ , Equation(1).

$$\Gamma = \{(x, y) | \varphi(x, y) = 0\}, \quad (1)$$

The level set function φ takes negative values inside the region of Γ and positive values outside [15]. It is able to satisfy the level set equation if Γ curve could move in the normal direction with speed v . The relation between level set function and level set equation is illustrated in Equation(2).

$$\frac{\partial \varphi}{\partial t} = v |\nabla \varphi|. \quad (2)$$

The work presented in [13] used level set method for image and volume segmentation of AAA. This method was used in order to define the static and evenly spaced mesh in the image or volume [13]. As previously mentioned, the values of each point in the mesh are based on the value of evolving curve, (Γ curve). The points within the Γ curve were given negative value while the points outside the curve were positive value. The mesh values then were updated using the speed function (Level set equation). This equation is shown in Equation (3) [13]. In this equation (3), φ_t is a matrix of mesh values at time t , F is the speed function and ∇ is a suitable spatial difference operator.

$$\varphi_{t+1} + F |\nabla \varphi_t| = 0 \quad (3)$$

In general, a speed function can be dependent on several factors, these factors in segmentation applications can be an *Advection* term which is a constant value, a curvature term based on the zero level set and last term based on image or volume (Concerning the edges of the shape)[13]. The second and third factors, curvature and image force are considered in accordance to the zero level set only. These values should be calculated for each mesh point, the mesh update should be considered as well. To solve this problem the value at any given mesh point is defined based on the value of the nearest point in the zero level

set. The proposed approximation in order to find the value of the two terms is computationally expensive. Due to this reason the authors proposed to use the narrow band with the level set method. This option reduced the computational cost by updating the mesh in an area restricted to the zero level set. In this method the mesh is updated after few steps with respect to time while the zero level set is accessing the points which were not updated [13]. The proposed 3D level set method in [13] was used to represent the 2D surfaces in 3D space [13]. In order to use the level set method the speed function was defined based on volume data from CT images, which is expressed in Equation 4. Term F is the force at the mesh point x, y , F_0 is the Advection force which was set to unity in all the experiments, F_c is curvature term which is calculated for the nearest point to x, y , on the zero level set which is x', y' and finally F_i is the image force based on the Gaussian derivative filter. The Gaussian filter was chosen over Sobel or Canny edge detectors since it provides better performance in detecting the weaker edges, it also allows to detect edges in the exact direction.

$$F(x, y) = (F_0 \nabla \varphi_{x,y} + F_c(x', y') \nabla \varphi_{x',y'}) e^{-F_i(x', y')} \quad (4)$$

As it was mentioned previously, the narrow band update was used to reduce the computation cost, more over updating only a section of the level set, e.g. 5 slices per time, made the calculation much more efficient [13]. The order of updating section was obtained using two methods. In the first method the first slices will be selected from one end of the mesh, e.g. top. The update is calculated for this set of slices until the changes in the mesh in accordance to the zero level set falls below a threshold. The same procedure will be repeated for the next set of slices [13]. In the second method the area of the mesh is changing constantly in order to grow the segmented area evenly [13]. The first method could be used for faster computation; however the second method provides better segmentation [13].

In addition to the mentioned concepts the authors also used multi resolution analysis (MRA). The implemented method used the volume data to produce the half resolution in all the directions. The mentioned method then is applied first to the low resolution data. The top down approach was considered for segmenting the data considering the computational cost into account. In the next step the obtained result from low resolution data were scaled up and were used as the starting point for the algorithm to run on the full volume data set [13]. The MRA also improves the computational cost from days to hours on a single processor machine. It should be considered that the proposed algorithm could be further speeded up using multi-processor machines [13].

In the next stage the 3D triangulation surface was formed. The Marching Cubes algorithm was used to

produce the iso - surfacing with zero value [13]. The visualization method, iso-surface is a surface that represents points with the constant value, in this case, velocity within a volume of space. In other words, it represent the level set of continuous speed function within 3D space [16]. Marching cubes is a popular method for constructing the iso-surface from a volume data [16]. This algorithm is using the scalar field, by considering eight neighbour locations per time. These eight points provide the imaginary cube. In the next step a plane figure bounded by the closed path (polygons) which is representing the part of the iso-surface passing through this cube is obtained. The individual polygons then will be joined together in order to obtain the desired surface [17]. Figure 4 shows the example of triangulations formed using this method. This method provides the accurate measurement which are currently measured inaccurately in the slice plane.

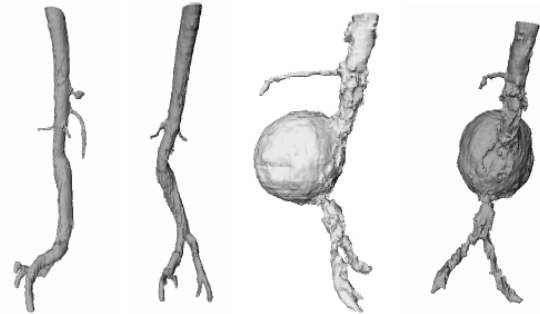


Fig. 4: Triangulated surface of the zero level set using the marching cubes algorithm

The level set method over previous proposed method has the advantage to provide better and more accurate results especially in segmenting small features; however the computational cost is quite high, even with the mentioned considerations. Due to this fact the author suggests to combine this method with other methods. This means to provide the initial segmentation with faster implementation and improve this segmentation using the level set method, considering the segmented data only. This will allow for faster and more accurate results.

B. AAA Segmentation Using Active Shape Models

As presented in previous sections, the aortic diameter is an important characteristic that should be evaluated in order to diagnose AAA. A way to detect this malformation is to compute a 3D reconstruction of the aorta to estimate location and risks of rupture. After acquiring a set of 2D CT transverse slices, the aorta can be segmented on each slice which will allow a three dimensional reconstruction. A family of methods based on shape segmentation can be used in order to solve the aorta reconstruction issues.

Kass et al. proposed a method called "Snake" or

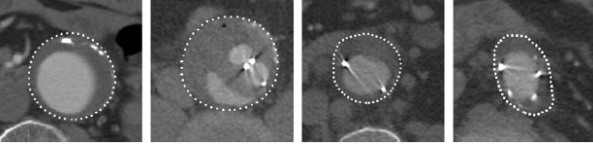


Fig. 5: Four CT slices where the aorta is delimited manually by an expert (white dots).

Active Contour Models [12]. This method allows to fit a contour around the object. However, the *Active Contour Models* method suffers of different problems:

- It is dependent of the initial "Snake".
- It does not have a good performance when the objects which have to be segmented are occluded.

In order to solve the last point, Cootes et al. integrated a training phase to acquire pre-knowledge about the shape of the target object [10]. This method is called *Active Shape Models* (ASM) or "Smart Snake". The ASM method allows a balanced construction between data fitting and a consistence with the training set.

To apply ASM method on medical images, shapes proved not to be enough; therefore, Cootes et al. integrated a modelization of the grey level appearance [8]. Bruijne et al. proposed an extension of the last method where they combined the grey level appearance with similarity of the adjacent slice [7].

1) Shape Modelling:

- Training Data Set:
The first step to model the shape of the aorta is to acquire images and manually label them, as shown in Figure 5 [7].
- Shape Alignment:
All shapes are defined in different reference axes. They have to be first aligned in the same reference axis in order to construct a general model. Procrustes Analysis can achieve this task as proposed in [9]. The Procrustes Analysis minimizes the distance between a reference shape and each of the remaining shapes in the dataset.
- Statistics Computation of Aligned Shapes:
Once all shapes have been aligned, statistics can be computed in order to model the shape variations. Each shape x can be decomposed using an eigen decomposition. x can be decomposed as a sum of a mean \bar{x} and a linear combination of eigenvectors Φ :

$$x = \bar{x} + \Phi b \quad (5)$$

Φ can be considered as a dictionary; this dictionary is built during the training phase and is based on eigen decomposition. The method to construct the dictionary is the following:

- Compute the mean shape using all the shapes as:

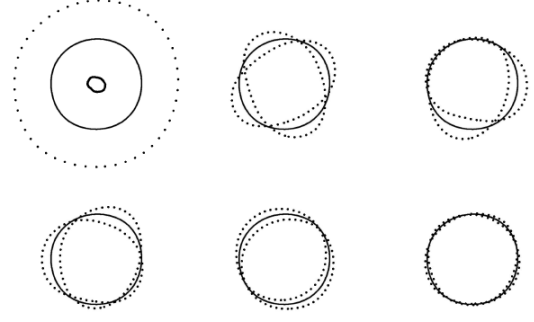


Fig. 6: Deviation compare to the mean shape moving independently the six first coefficients of the vector \mathbf{b} . Solid line: mean shape. Dashed line: a variation of $\sqrt{\lambda_i}$.

$$\bar{x} = \frac{1}{N} \sum_{i=1}^N \quad (6)$$

where x_i is the i^{th} landmark of the shape.

- Compute the covariance matrix S as:

$$S = \frac{1}{N} \sum_{i=1}^N (x_i - \bar{x})(x_i - \bar{x})^T \quad (7)$$

- Compute the eigenvectors φ_i from the scatter matrix S . At this point, any shape x can be decomposed as:

$$x = \bar{x} + \Phi \mathbf{b} \quad (8)$$

where $\Phi = \{\varphi_1, \varphi_2, \dots, \varphi_n\}$.

- Sorting them and keeping the k eigenvectors corresponding to the largest eigenvalues λ_i . Only a few number of eigenvectors can be used to approximate each shape as:

$$x \approx \bar{x} + \Phi \mathbf{b} \quad (9)$$

where $\Phi = \{\varphi_1, \varphi_2, \dots, \varphi_k\}$.

- k is determined as:

$$\sum_{i=1}^k \lambda_i \geq f_v \sum_{i=1}^n \lambda_i \quad (10)$$

where f_v is a coefficient of approximation between 0 and 1. When $f_v = 1 \rightarrow \Phi = \{\varphi_1, \varphi_2, \dots, \varphi_n\}$. When $f_v = 0 \rightarrow \Phi = \{\emptyset\}$.

Figure 6 presents the deviation compared to the mean shape moving independently of the six first coefficients of the vector \mathbf{b} .

2) *Gray-level appearance modelling*: In order to localize the object, not only the shape of the object is important but also the appearance. In order to compute this model, a window is defined around each landmark of size $k_n \times k_t$ where n means normal to the edge and t means transversal to the edge. Values inside the

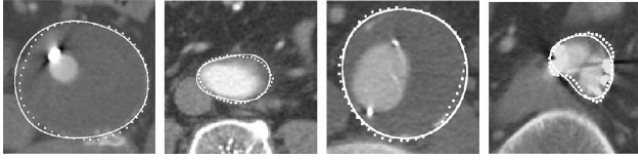


Fig. 7: Results using automatic segmentation. Dot line is the manual segmentation while the other is the automatic segmentation

window correspond to the first derivative of the image around the landmark considered; Bruijne presents several coefficients [7]. However, only coefficients giving the best results will be presented which is the sum of absolute intensity differences between sample and reference patches:

$$AD = \sum_{x=0}^{k_n \times k_t} |I_s(x) - I_r(x)| \quad (11)$$

where I_s is the sample image and I_r is the reference image. This coefficient is performed for several resolutions.

3) *Model fitting*: The initialization is done by drawing the shape by hand. Then for the adjacent slice, the previous contour found is used as initialization. In order to find new boundaries, a multiresolution analysis is performed from coarse to fine resolution to have more accuracy at each scale and find the sub motion. At each scale and for each landmark, the sample patch is moved along the normal and the sum of absolute intensity differences between sample and reference patches is computed (Equation (11)). The purpose is to minimize this coefficient. This operation is done N times or until that the coefficient is small enough. Once that the new shape is found, the vector \mathbf{b} can be computed as:

$$\mathbf{b} = \Phi^T(x - \bar{x}) \quad (12)$$

Results of this automatic segmentation are presented on the figure 7.

IV. MAGNETIC RESONANCE IMAGING MODALITIES

A. Gadolinium-enhanced MRI

Although MRI is an imaging modality that has been widely used to retrieve anatomical and physiological information of a patient, its use in vascular imaging is limited due to the flow artifacts generated in different pathologies; aneurysms usually present a slow, swirling flow, whereas in stenotic vessels the flow can be turbulent [2]. The injection of gadolinium, a paramagnetic contrast agent, to the patient's blood flow shortens the T1 relaxation time of blood, making it easier to distinguish it from the surrounding tissues. Prince et al. [2] reported a correct classification of aneurysms when experts were shown contrast-enhanced MR images; the size of the aneurysm measured on MR images was

within 3 mm of CT image measurements and within 5 mm of ultrasound measurements [2]. Figure 8 shows the agreement between the measured AAA size in each imaging modality. The character of the aneurysms was also appropriately identified: no false-positive or false-negative results for aortic rupture, aortic dissection or inflammatory aneurysms were determined from the MR images [2].

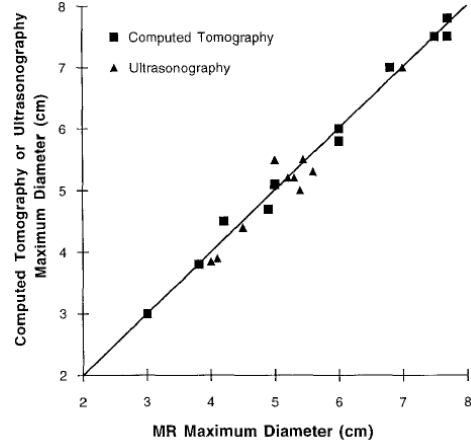


Fig. 8: MRA AAA diameter measurements versus CT (*square*) and ultrasound (*triangle*)

Figure 9 shows two gadolinium-enhanced images (A and C) and a conventional aortogram (B and D) of a abdominal aortic aneurysm. It can be seen that the blood vessels have a higher intensity value than the surrounding tissues; in Figure 9A) there is a major enhancement of the arteries with respect to the overlapping veins, due to the contrast agent flow. From these images it can be seen that there is an agreement between the anatomic characteristics found in the MR images and the aortograms. The whole aneurysm can be seen on a single large field-of-view image, which cannot be achieved using angiographic images because of the large concentrations of iodinated contrast agent that are required [2]. On the other side, gadolinium has the advantage of being safe to use in patients with renal insufficiency because it has no known side effects and no nephrotoxicity [2].

Therefore, it was concluded in [2] that gadolinium-enhanced MRA provides sufficient anatomic detail to detect all aneurysms. Still there exist some limitations, inherent to MR imaging, when wanting to image patients with pacemakers and other implants or when renal artery lesions are to be evaluated. Fortunately, gadolinium-enhanced MRA does not interfere with other imaging modalities, that can be done immediately afterwards, and is therefore an imaging modality that greatly serves for preoperative evaluation of AAA.

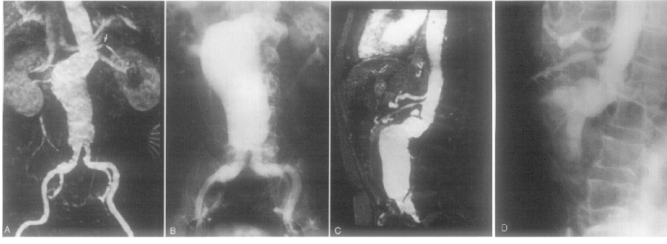


Fig. 9: **A.** Gadolinium-enhanced MRA **B.** Conventional Aortogram (Xray) **C.** Time of Flight MRA with Gadolinium-enhancement **D.** Conventional Lateral Aortogram

B. Diffusion-weighted MRI

Orta et al. reported the use of diffusion-weighted MRI to diagnose a particular type of aneurysm, inflammatory abdominal aortic aneurysm [1]. The MR contrast-enhanced images, where soft tissue surrounding the blood vessel appeared enhanced, suggested IAAA; but DW-MRI confirmed the diagnosis. DW images, that revealed a hyper-intensity surrounding the aorta, were of great importance to finally determine the inflammatory nature of the disease [1].

Figure 10 shows the imaging studies done to the patient [1]. Figure 10A) is a T1-weighted MR image that reveals an unusual enlargement of the spleen and a dilation of the abdominal aorta, as shown by the arrows. The inflammatory nature of the disease is depicted by the enhancement of the soft tissue after contrast injection in Figure 10B). These findings were confirmed using DW-MR imaging, where the inflammatory tissue is shown by the arrows as a high-intensity region in Figure 10C). Finally, Figure 10D) shows the region where the ADC was computed; it yielded a value of $1.24 \times 10^{-2} mm^2/s$, which is consistent with a restricted diffusion due to inflammation.

It can therefore be concluded that DW-MRI is an imaging modality that can be used to study abdominal aortic aneurysms, it has the advantage of being able to quantitatively determine the inflammatory nature of the aneurysm [1]. In conjunction with US, CT or MRI, it can help determine the appropriate preoperative management and surgery planning.

V. MR IMAGE PROCESSING

Once the images have been acquired and AAA is suspected, appropriate image post-processing methods should be chosen in order to aid the physician emit a diagnosis. In an AAA disease, it is important quantitatively measure the vessel diameter; automatically detecting the aortic contours would be a first step in segmenting the vessel to then proceed to a diameter measurement. This section presents two segmentation methods applied to MR images. The first method is a Markovian method evolving into an implicit contour segmentation method, whereas the second method

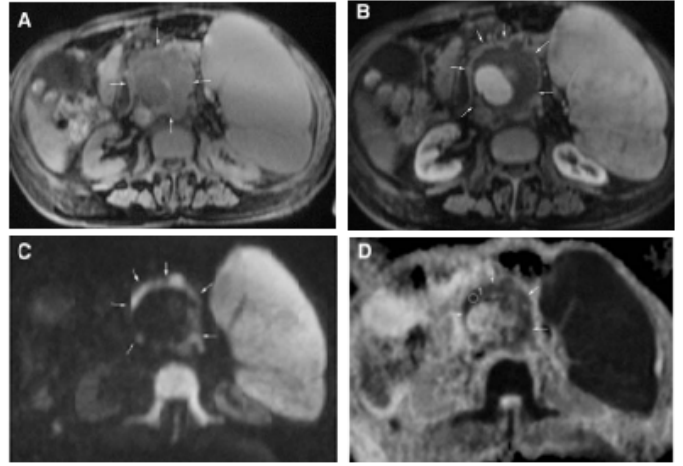


Fig. 10: Axial MR Images of IAAA. **A.** Fat-saturated T1 image **B.** Post-contrast fat-saturated T1 image **C.** Diffusion-weighted image **D.** ADC computation on ROI on aortic wall

was based on a graph-based image segmentation approach.

A. Markovian Method for Aortic Segmentation

Jodoin et al. presented in [3] a Markovian method that evolves into an implicit active contour segmentation method. This method minimizes an energy function that allows for a simple and fast Markov Random Field implementation while including a parameter for curve smoothness that achieve a level-set-like active contour evolution. Given two random fields modelling the segmentation labels and the input image, X and Y with realizations x and y , the grey scale feature of y is used to compute x such that pixels with similar intensity values are grouped in the same class [3]. The criterion for segmentation is the Maximum a Posteriori Probability (MAP) given by $x' = \operatorname{argmax}_x \left(\frac{P(y|x)P(x)}{P(y)} \right)$ [3]. Assuming they are all Gibbsian distributions, then the MAP is given by Equation 13, where U is the likelihood energy function and V is the prior energy function.

$$x' = \operatorname{argmin}_x \sum_{s \in S} U(x_s, y_s) + V_{\eta_s}(x_s) \quad (13)$$

The likelihood energy function is taken to be the natural logarithm of a Gaussian and the prior energy function that is evaluated and minimized in shown in Equation 14.

$$V_{\eta_s}(x_s) = \alpha \left(\frac{\operatorname{card}(\eta_s)}{\sum_{t \in \eta_s} \delta(x_s, x_t)} - 1 \right) \quad (14)$$

Here, x represents the segmentation label, η_s the number of neighbours of site s and $\delta(x_s, x_t)$ is the Kronecker delta that returns 1 when $x_s = x_t$ and 0 otherwise. Therefore, a pixel s will switch classes if and

only if at least one of its neighbours has already been assigned the new class label [3]. This is exemplified in Figure 11; Figures 11 A) and 11 C) show the initial contours and label fields of the image. Because points c and d are located in uniform regions, their labels will not change; on the other hand, points a and b , located near a boundary, will change their labels and will cause the regions to grow or shrink in order to adapt to the image contours.

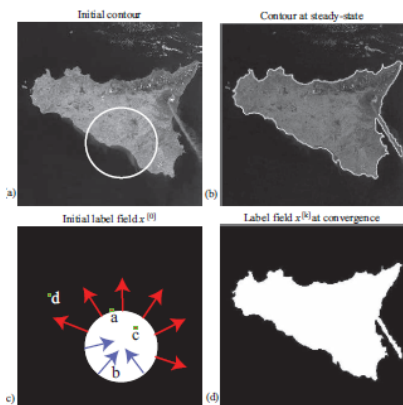


Fig. 11: **A.** Contour Initialization. **B.** Final Contour. **C.** Initial Label Field **D.** Final Label Field

Extension from a two-dimensional segmentation to a three or four dimensional one is relatively simple and greatly depends on the definition of the neighbourhood η_s . For a 3D segmentation, neighbours are located in the current analysed image, k , and on the stack images $k-1$ and $k+1$. The extension to 4D is done by including neighbours on temporally adjacent stacks of images, i.e. image stacks at times t , $t-1$ and $t+1$. Also, in order to account for the different grey scale distributions of each image stack, a mixture of two Gaussians was associated to each image stack; each class would then be linked to time-dependent Gaussian mean and standard deviation parameters [3]. Figure 12 shows the result of a three-dimensional segmentation of the abdominal aorta and the vessel reconstruction on the leftmost side; the initialization was done manually by a physician on the first image of each stack. As can be visually evaluated from the the right-hand images, the algorithm accurately segments the blood vessel. Figure 13 depicts the extension of the algorithm to four dimensions, also accurately segmenting the aorta at different time frames.

As could be seen from the results, the method was able to accurately segment the blood vessels. Further steps in assessing AAA disease could include the determination of a maximum lumen diameter and a comparison with predefined diameter ranges in order to plan the appropriate treatment or surgery.

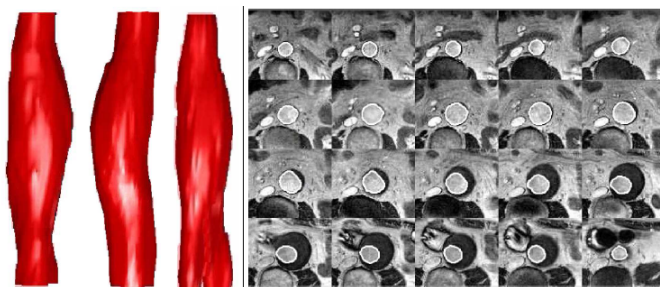


Fig. 12: Results for 3D Segmentation and Wall Vessel Reconstruction

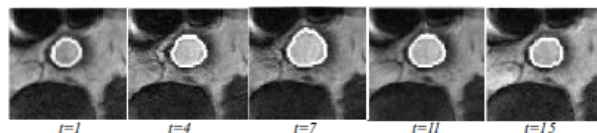


Fig. 13: Results for 4D Segmentation at Different Time Frames

B. A Graph-Theoretic Approach for Aortic Segmentation

Sonka et al. implemented a pre-segmentation algorithm consisting of a fast marching level set method on four-dimensional MR aortic images to obtain an approximation of the aortic surface [3]. From these results, a center line was computed by skeletonization of the surfaces. Finally, through a novel 4D border detection algorithm, an accurate blood vessel surface segmentation was achieved.

The algorithm implemented by Sonka et al. was based on a graph-based image segmentation approach [5]. Here, a weighted graph $G = (V, E)$ represents the image pixels as nodes in set V and the neighbourhood system in an arc set E ; there is an inherent cost function in each arc $\langle v_i, v_j \rangle$. Graph-cuts aim to partition a weighted graph into two disjoint subsets [5]. They minimize the cost function, $\epsilon(f)$, through the design of node sets G_{st} containing *source*, s , and *sink*, t , label nodes. With an appropriate design of an energy function, a minimum $s-t$ cut can segment a region of interest in an image [5].

Graph-based image segmentation proved to accurately segment vascular contrast-enhanced MR images; Figure 14 A) shows the original images, Figure 14 B) the manual segmentation and Figures 14 C) and D) the automatic segmentation.

The algorithm's performance was evaluated by comparing the results with those of manual segmentation done by a physician. Figure 15 shows the mean and standard deviation values for the positioning errors of the segmentation; the error was defined as the shortest distance of the automatic and the manual segmentation [4].

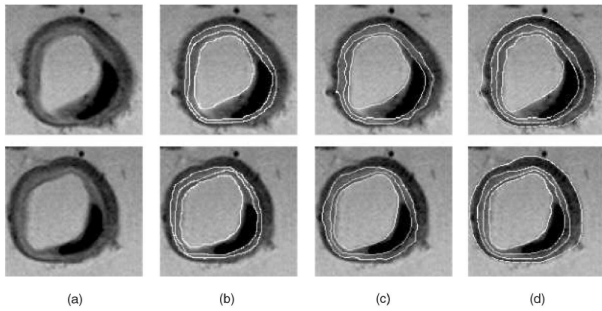


Fig. 14: Segmentation of MR arterial walls and plaque

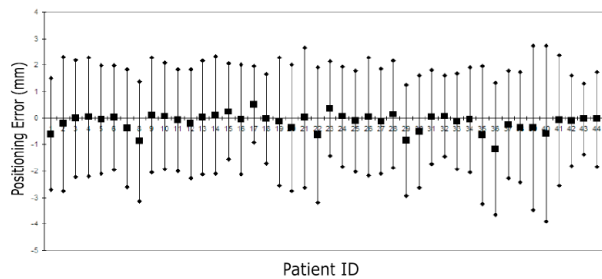


Fig. 15: Positioning Errors for Aortic Segmentation

VI. CONCLUSIONS

As has been shown in the previous sections, there is a strong interest in exploiting the capabilities of the medical imaging modalities to diagnose abdominal aortic aneurysm. The choice of the imaging modality is the first step that should be considered in order to study AAA; CT and MRI are important imaging modalities that provide anatomical details of the diseased vessel. Currently, the modality of choice in most institutions is CT with an iodinated contrast medium, especially in emergency patients. Though it is useful to show the vessel anatomy, MRI has proven to be more reliable when wanting to detect inflammatory changes in the lesion. They are both non invasive imaging techniques but CT makes use of ionizing radiation and employs a contrast agent inappropriate for patients with renal insufficiency. A diagnose based on both CT and MR images will probably be a more accurate one as the anatomical and physiological information of the disease will be complemented.

After the appropriate images are shown there are several post-processing techniques that aim to aid the physician to diagnose AAA. Most of these methods rely on segmentation of the aorta and a later measurement of the vessel diameter. Level sets and active shape model methods have been used with good results in CT images; Markovian and graph-theoretic approaches have been developed for MR images. Either of these methods could be extended to the other modality, though not much research has been done on it. It would be interesting to perform a study in which the several segmentation methods are used on CT and MR in order

to evaluate the methods and the imaging modalities in a better way.

VII. REFERENCES

- [1] Orta, K. and Kilickesmez, O. Clear Depiction of Inflammatory Abdominal Aortic Aneurysm with Diffusion-Weighted Magnetic Resonance Imaging. *Cardiovascular and Interventional Radiology*. (2010) 33:379-382.
- [2] Prince, M. et al. Gadolinium-enhanced Magnetic Resonance Angiography of Abdominal Aortic Aneurysms. *Journal of Vascular Surgery*. (1995) Volume 21. Number 4.
- [3] Jodoin, P. et al. Markovian Method for 2D, 3D and 4D segmentation of MRI. (2008) 15th IEEE International Conference on Image Processing.
- [4] Sonka, M. et al. Early Detection of Aortic Aneurysm Risk from 4D MR Image Data. (2006) *Computers in Cardiology*.
- [5] Kang Li et al. Optimal Surface Segmentation in Volumetric Images - A Graph-Theoretic Approach (2006) *IEEE Transactions on Pattern Analysis and Machine Intelligence*. Volume 28. Number 1.
- [6] Crawford, C. et al. Abdominal Aortic Aneurysm: An Illustrated Narrative Review. (2002) *Journal of Manipulative and Physiological Therapeutics*. Volume 26. Number 3.
- [7] Marleen de Bruijne and Bram van Ginneken and Max A. Viergever and Wiro J. Niessen. *Interactive Segmentation of Abdominal Aortic Aneurysms in CTA Images*. 2004.
- [8] T.F. Cootes and A. Hill and C.J. Taylor and J. Haslam and Manchester M Pt. *The Use of Active Shape Models For Locating Structures in Medical Images*. 1994.
- [9] T.F. Cootes and C.J. Taylor and Manchester M Pt. *Statistical Models of Appearance for Computer Vision*. 2000.
- [10] Cootes, T. F. and Taylor, C. J. and Cooper, D. H. and Graham, J. *Active shape models - their training and application*. *Comput. Vis. Image Underst.* 1995. Volume 61. Issue 1. Pages 38-59.
- [11] A. Hill and A. Thornham and C. J. Taylor. *Model-Based Interpretation of 3D Medical Images*. In *British Machine Vision Conference*. 1993. BMVA Press.
- [12] Michael Kass and Andrew Witkin and Demetri Terzopoulos. *Snakes: Active contour models*. *International Journal of Computer Vision*. 1988. Volume 1. Number 4.
- [13] Derek Magee and Andrew Bulpitt and Elizabeth Berry. *Level Set Methods for the 3D Segmentation of CT Images of Abdominal*.
- [14] Steven C. Mitchell and Boudewijn P. F. Lelieveldt and Rob J. van der Geest and Hans G. Bosch and Johan H. C. Reiber and Milan and Milan Sonka. *Multistage Hybrid Active Appearance Model Matching: Segmentation of Left and Right Ventricles in Cardiac*

MR Images. IEEE Transactions on Medical Imaging. 2001. Volume 20.

[15] Wikipedia. Level Set Method. December 2010. http://en.wikipedia.org/wiki/Level_set_method

[16] Wikipedia. Isosurface. December 2010. <http://en.wikipedia.org/wiki/Isosurface>

[17] Wikipedia. Marching Cubes. December 2010. http://en.wikipedia.org/wiki/Marching_cubes

[18] George G. Hartnell. FRCR, FACC. Imaging of Aortic Aneurysm and Dissection: CT and MRI. Journal of Theoretical Imaging. 2001.